Sensors and Materials, Vol. 35, No. 5 (2023) 1701–1714
MYU Tokyo

S & M 3281

State of Charge Estimation of Electric Vehicle Power Batteries Enabled by Fusion Algorithm Considering Extreme Temperatures

Mingcan Xu[1] and Yong Ran[2*]

[1]Chongqing Three Gorges Vocational College, Chongqing 404155, China
[2]School of Intelligent Manufacturing, Chongqing Three Gorges Vocational College, Chongqing 404155, China

(Received January 7, 2023; accepted April 3, 2023)

Keywords: energy harvesters, charging state, adaptive extended Kalman filter, long-term and short-term memories, estimation accuracy

When using the extended Kalman filter (EKF) to estimate the state of charge (SOC) of lithium-ion batteries (LIBs), the noise covariance matrices of system and observation noises for energy harvesters are mostly given randomly, which makes it impossible to optimize the noise problem. This results in the low accuracy and stability of SOC estimation. To address these problems, a method of estimating the SOC of power LIBs based on long short-term memory–adaptive unscented Kalman filter (LSTM–AUKF) fusion is proposed to improve the accuracy and stability of estimating the SOC of LIBs. First, the offline parameters of the Thevenin model are identified from the hybrid pulse power characterization (HPPC) experimental data. Then, the LSTM structure of the SOC estimation window is constructed for power LIBs, and the power battery SOC training network is predicted in real time from the power battery current, voltage, temperature, and historical data. Finally, the AUKF algorithm for estimating the SOC of power LIBs is designed, then a fusion strategy is proposed. The experimental validation shows that the root mean squared error (RMSE), maximum (MAX), and mean absolute error (MAE), used to estimate the SOC of the LSTM–AUKF hybrid power lithium battery in the research window, are 1.13, 1.74, and 0.39%, respectively. Compared with the window LSTM network, the fusion algorithm improves the accuracy and stability of SOC estimation for power LIBs.

1. Introduction

With the gradual acceleration of national strategic processes, for example, energy substitution and the promotion of large-scale new energy consumption, lithium-ion batteries (LIBs) have been used in many scenarios because of their high efficiency as energy storage devices.[1,2] According to the statistical analysis results of the Starting Point Research Institute, the total shipment of LIB worldwide increased by 34% year-on-year in 2020, reaching 259.5 GW·h. Global shipments of LIBs are expected to reach 1.1 TW·h by 2025.[3] With the growing global market for LIBs, related supporting technologies such as state of charge (SOC) estimation must be improved to ensure the popularization and application of LIBs in multiple scenarios. The

*Corresponding author: e-mail: xumc107@163.com
https://doi.org/10.18494/SAM4319

ISSN 0914-4935
https://myukk.org/

modeling of power batteries is the basis of SOC estimation, and its importance is self-evident. Equivalent circuit models, such as the Partnership for a New Generation of Vehicles (PNGV), Rint, and Thevenin models, simulate the external characteristics of a circuit network composed of a series of resistors, capacitors, and constant voltage sources.

SOC estimation, as one of the main functions of a battery management system (BMS), plays an important role in different applications. For example, in the application of electric vehicles, accurate SOC estimation is crucial in preventing them from overcharging or depleting power and prolonging the battery life. Furthermore, it can promote the industrialization of the process of developing electric vehicles.[4,5] For consumer electronic products, the accurate estimation of the SOC of LIBs will help users flexibly manage the remaining available time of the battery of electronic products and improve user comfort and convenience.[6,7] In energy storage power plants, SOC, an important reference indicator for the safety protection of LIB energy storage systems, plays a significant role in maintaining the stable operation of the system and ensuring the safety of personnel.[8] If the SOC of a LIB energy storage system is not accurately estimated, it may lead to overheating, burning, and other accidents of the energy storage battery, and ultimately endanger the safe and stable operation of the energy storage plant and even the power system. Therefore, methods of estimating the SOC for LIBs have become an important topic in battery research.

In practical applications, the SOC of LIBs is affected by many factors such as the charging and discharging currents, the ambient temperature, and self-discharging. It is impossible to obtain precise values of the SOC directly. Therefore, for the high-precision estimation of the SOC, it is necessary to conduct a comprehensive analysis of various factors that affect the SOC. SOC estimation methods for LIBs can be summarized into four types: experiment-based,[9] model-based,[10] data-driven,[11] and fusion-based.[12] The first type mainly accurately estimates the SOC by measuring battery characterization parameters through experiments. The second type estimates the battery SOC by designing an equivalent circuit model of the battery. The third type estimates the SOC of the battery by fitting many data and using empirical methods and mathematical models. The last type of method, learning from the existing types and integrating them to improve the accuracy and efficiency of SOC estimation, is currently a research hotspot.

The main contributions of this paper are as follows: (1) We study the SOC estimation of an N18650CK power lithium battery and propose a fusion algorithm that couples improved particle swarm optimization, i.e., LSTM, with the AUKF algorithm. The changes in voltage upon battery pulse charging and discharging are obtained under hybrid pulse power characterization (HPPC) operating modes, and the impedance parameters of the battery are identified using Ohm's law. (2) The impedance parameters of the battery are identified by using Ohm's law in combination with the changes in voltage upon the pulse charging and discharging of the battery under HPPC operating conditions, and then an LSTM power battery estimation model is constructed. (3) The experimental validation shows that the root mean squared error (RMSE), maximum (MAX), and mean absolute error (MAE), used to estimate the SOC of the LSTM–AUKF hybrid power lithium battery in the research window, are 1.13, 1.74, and 0.39%, respectively. Compared with the window LSTM and LSTM–EKF networks, the fusion algorithm considering extreme temperatures improves the accuracy and stability of SOC estimation for power LIBs.

2. Establishment of Battery Model

2.1 Analysis of battery equivalent model

An effective battery model is a basis for the accurate estimation of the SOC. Wu *et al.* found that the second-order RC equivalent circuit model can effectively reflect the physical and chemical changes in the battery at a low calculation cost,[13] which meets the requirements of a BMS. Therefore, the Thevenin second-order equivalent circuit model illustrated in Fig. 1 is used.

The double parallel RC links are used to simulate the hysteresis effect caused by the electrochemical and concentration polarizations of the lithium battery. The internal resistance of the power lithium battery is R_0 and the electrochemical and concentration polarization internal resistances are R_1 and R_2, respectively. The open-circuit voltage (OCV) electromotive force is E_t, the observation terminal voltage is U_d, and the battery electrochemical pole and concentration polarization voltages are U_1 and U_2, respectively. The electrochemical and concentration polarization capacitances are C_1 and C_2, respectively, the available capacity of the battery is Q_n, the working current of the battery is I_d, the charge–discharge efficiency is η, the operation time is t, and the current SOC is SOC(t). According to Thevenin's theorem, a system of state transfer equations for power batteries can be obtained as follows.

$$i(t) = \frac{U_1(t)}{R_1} + C_1 \frac{dU_1(t)}{dt} = \frac{U_2(t)}{R_2} + C_2 \frac{dU_2(t)}{dt} \tag{1}$$

$$SOC(t) = SOC(0) - \eta \frac{\int_{\tau=0}^{t} i(\tau) d\tau}{Q_n} \tag{2}$$

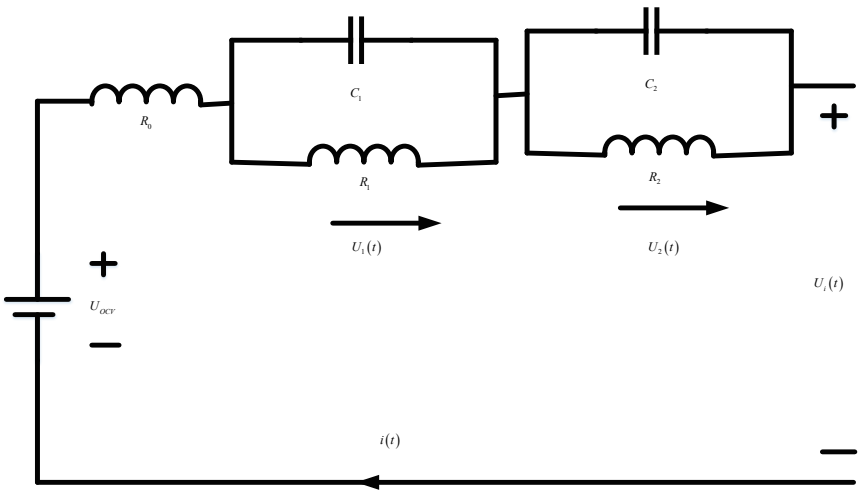

Fig. 1. Thevenin second-order RC equivalent circuit model.

$$U_i(t) = U_{OCV} - U_1(t) - U_2(t) - R_0 \cdot i(t) \tag{3}$$

For further discretization of Eqs. (1)–(3), we set the sampling interval as ΔT to obtain

$$i(k) = \frac{U_1(k)}{R_1} + C_1 \frac{U_1(k+1) - U_1(k)}{\Delta t} = \frac{U_2(k)}{R_2} + C_2 \frac{U_2(k+1) - U_2(k)}{\Delta t}, \tag{4}$$

$$SOC(k) = SOC(k-1) + \eta \frac{\Delta t}{Q_n}, \tag{5}$$

$$U_i(k) = U_{OCV} - U_1(k) - U_2(k) - R_0 \times i(k). \tag{6}$$

2.2 Identification of battery model parameters

In the equivalent circuit model, the SOC–OCV characteristic curve of the battery model can only be determined only after R_0, R_1, R_2, C_1, and C_2 are determined. The system uses an N18650CK power lithium battery with a rated capacity of 30 Ah. In this study, a constant-current pulse discharge is used to identify battery parameters.[14]

The experiment is carried out under the condition that the ambient temperature is kept at 25 ℃. In the experiment, discharge occurs at a rate of 1 C per 15 min, then the equipment is left to stand for 40 min. The SOC and OCV values obtained by the experiment are fitted by the CFTOOL tool in MATLAB, and the best fit is obtained using a fifth-order polynomial. Figure 2 shows the SOC–OCV characteristic curve.

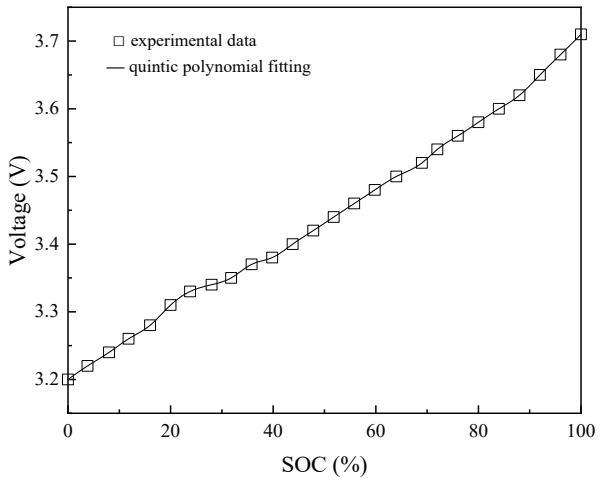

Fig. 2. SOC–OCV fitting curve.

The fifth-order polynomial of the SOC–OCV characteristic curve is defined as

$$U_{OCV} = 23.15 \cdot SOC^5 + 18.69 \cdot SOC^4 - 6.275 \cdot SOC^3 - 152 \cdot SOC^2 + 1.28 \cdot SOC + 2.24. \quad (7)$$

The parameters R_0 and RC in the internal resistance of the model should be identified in combination with the response process of the pulse discharge under different SOCs. Figure 3 is the voltage response diagram of a pulse discharge, where $A \rightarrow B$ is the static state, $B \rightarrow D$ is the discharge process, and $E \rightarrow F$ is the zero-state response of the voltage at the end of the discharge. For the charge process shown in Fig. 3, we have the following equations.

$$\begin{cases} R_0 = U_{ED}/I \\ U_i(i) - U_{OCV} = k_1 e^{-\lambda_1 t} + k_2 e^{-\lambda_2 t} \\ R_1 = k_1/I; R_2 = k_2/I \\ C_1 = \dfrac{1}{\lambda_1 R_1}; C_2 = \dfrac{1}{\lambda_2 R_2} \end{cases} \quad (8)$$

3. SOC Estimation Method Based on LSTM–AUKF Fusion

The two main implementation steps of the LSTM–AUKF fusion algorithm are as follows. (1) Build a window LSTM-based SOC estimation network for power LIBs and optimize the structure and parameters. (2) Build equivalent circuit models, design the AUKF algorithm and window LSTM network, and design the fusion strategy.

3.1 SOC prediction network based on window LSTM

Since the measured data (terminal voltage U_d, working current I_d, and surface temperature T_d) and output SOC of the power lithium battery are related to the historical data and current

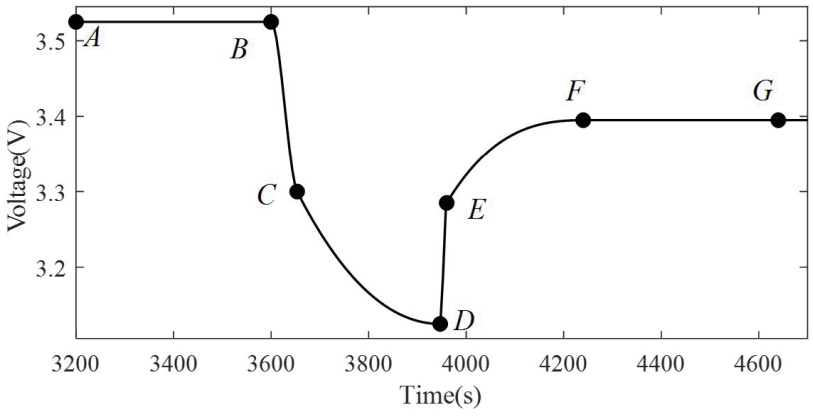

Fig. 3. One complete pulse discharge process.

state, a deep learning network with a circular structure is suitable for SOC estimation.[15] The LSTM network has the characteristics of transmitting the current and memory states.[16] Compared with the static neural network, a cyclic structure containing LSTM nodes is more helpful in extracting the characteristics of the battery time series. Figure 4 shows the architecture of the SOC estimation algorithm for power LIBs in the LSTM window network. A power battery SOC estimation algorithm framework for the window LSTM network is constructed on the basis of the characteristics of the battery input and output data and the LSTM nodes. We use the window LSTM loop neural network, which mainly consists of four parts, the input, circular, fully connected, and output layers, to estimate the SOC of a power lithium battery. The terminal voltage U_d, working current I_d, and surface temperature T_d are used as inputs, and the output is the SOC of the power lithium battery.

The recursive length is set as L_R, the number of hidden nodes in the network is N_h, and the estimated value at iteration k is SOC_k^{LSTM}. The terminal voltage $U_d(k)$, current $I_d(k)$, and temperature $T_d(k)$ of the power battery are measured at the k-time moment. The input vector $x(k)$ of the power battery at the k-time moment is $[U_d(k), I_d(k), T_d(k)]^T$. The standardized input vector is $x'(k)$. The window LSTM network input matrix $\chi(k)$ and the network output value $\gamma(k)$ are defined as

$$\chi(k)=\left[x'(k-\lambda+1),x'(k-\lambda+2),\cdots x'(k)\right]. \tag{9}$$

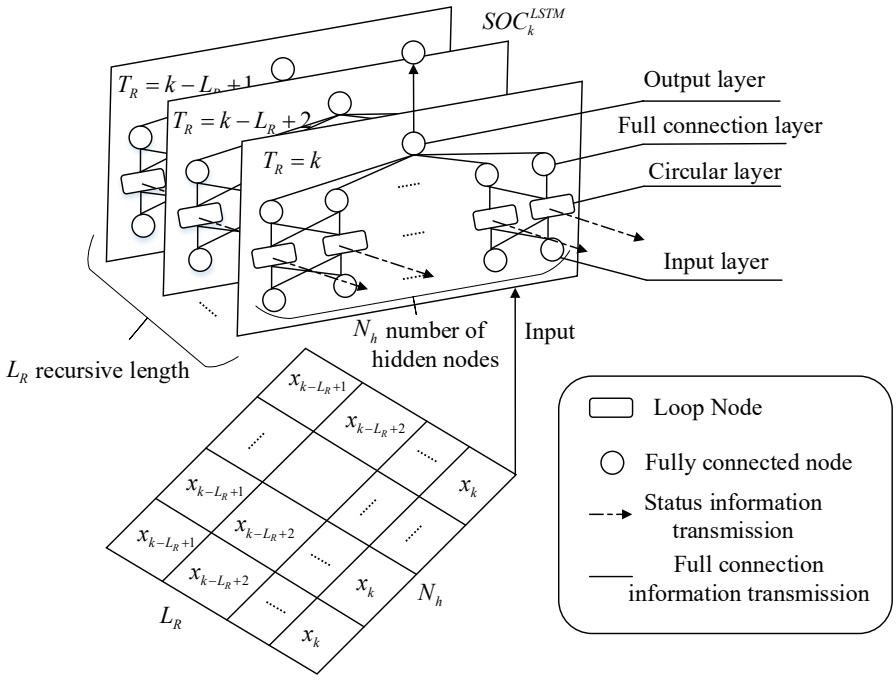

Fig. 4. Architecture diagram of SOC estimation algorithm for power LIBs in window LSTM network.

Here, each node in the fully connected layer is connected to the output of the cyclic node in the circular layer, and the time series feature information in the cyclic network layer is extracted. The number of nodes is $L_R \times N_h$. The output layer is a single node that outputs SOC_k^{LSTM}, which is predicted from the SOC at time k. The input layer is a fully connected node, and the number of nodes in the input layer is $L_R \times N_h$. Fully connected nodes receive input vector information at each time. The loop layer consists of multiple loop nodes. We set the number of hidden nodes in the network to N_h and the recursive length of the loop to L_R. At the same time, to improve the accuracy of the network, the generalization ability and convergence speed of the algorithm should be improved via data standardization and grouping, loss function optimization, and hyperparameter optimization.[17]

3.2 AUKF-driven estimation algorithm

The state and observation vectors at time k in the system state equation are set to X_k and Y_k, respectively; the input variable at time k is u_k. Moreover, the system, control, observation, and feedforward matrices are H, I, K, and M, and the process and measurement noises are $\alpha(k)$ and $\beta(k)$, respectively. Therefore, the discretized expressions for the state transfer and observation equations of the system are respectively defined as

$$X_k = H \cdot X_{k-1} + I \cdot u_{k-1} + \alpha(k), \tag{10}$$

$$Y_k = K \cdot Y_{k-1} + M \cdot u_{k-1} + \beta(k). \tag{11}$$

We set the expectation of state quantity X_k at time k as $\overline{X}_{k|k}$ for the AUKF algorithm and the dimension of the state quantity as n_σ. We let the distribution of $2n_\sigma + 1$ points form matrix $X_{k|k}^\sigma$, then the observation quantity Y_k^σ of $X_{k|k}^\sigma$ can be calculated using Eqs. (10) and (11). The error covariance matrix at time k is $P_{k|k}$, then $X_{k|k}^\sigma$ is expressed as

$$X_{k|k}^\sigma = \left[\overline{X}_{k|k}, \overline{X}_{k|k} + \sqrt{(n_\sigma + \lambda) P_{k|k}}, \overline{X}_{k|k} - \sqrt{(n_\sigma + \lambda) P_{k|k}} \right]. \tag{12}$$

The noise of the system model is unknown and changes over time. Therefore, the Sage–Husa adaptive algorithm is introduced into the AUKF algorithm, which updates the noise parameters q_k, Q_k, r_k, and R_k in the UKF algorithm in real time to improve the accuracy of SOC estimation. The distribution formed by the $2n_\sigma + 1$ points achieves forward recursion, and the forward recursive state variable $X_{k+1|k}^\sigma$and observation $Y_{k+1|k}^\sigma$are obtained as

$$\begin{cases} X_{k+1|k}^\sigma = H \cdot X_{k|k}^\sigma + I \cdot u_k \\ Y_{k+1}^\sigma = K \cdot X_{k|k}^\sigma + M \cdot u_k \end{cases}. \tag{13}$$

3.3 LSTM forecast and AUKF strategy fusion

This section presents a fusion strategy to optimize the accuracy and stability of SOC estimation for power LIBs by analyzing the characteristics of the LSTM depth network and AUKF algorithm.

3.3.1 LSTM network prediction and AUKF algorithm characteristics

The window LSTM deep learning network is used to estimate the SOC of LIBs. It can extract multi-time slice information features, but it uses open-loop forward transmission without feedback correction. When the battery is aging or the internal resistance increases, the SOC estimations are prone to large errors. In practice, the estimated values fluctuate frequently. In contrast to the EKF algorithm, the AUKF algorithm is based on one-step prediction, it is a one-step correction method, and it uses the mean value of the σ-sampling point set of $2n_\sigma + 1$ state variables in the unscented transform in the equivalent circuit model mapping to replace the prior recursive state of the EKF. This is helpful for reflecting the probability density distribution of state variables after nonlinear mapping. However, if the AUKF algorithm is used to estimate the SOC of a powerful lithium battery, the following problems may also exist. (1) In the case of complex working conditions, i.e., large and frequent changes in input information, the AUKF algorithm is prone to generating large estimation errors of the SOC so that the algorithm does not converge. (2) When the error of the initial value of the SOC is large, the algorithm easily becomes nonconvergent or the covariance matrix cannot be decomposed.

3.3.2 LSTM network training and filtering algorithm fusion

To improve the fusion effect of the window LSTM network and AUKF algorithm, two optimization strategies are proposed. Figure 5 shows the integration strategy of the window LSTM network and AUKF algorithm, which includes two steps: (1) the window LSTM network is used to estimate SOC_k^{LSTM}. (2) Cholesky decomposition and adjustment, i.e., Cholesky decomposition adjustment, are used to improve the fusion effect.

4. Operation Mode Test and Experimental Analysis

4.1 Test platform and experimental objects

In this study, an N18650CK power lithium battery is used as the research object. The main performance parameters of a single battery are shown in Table 1. A test platform is set up to test the battery under various operating modes. The platform consists of a thermostat, a battery test device, and a computer, as shown in Fig. 6. The thermostat can provide a range of test temperatures of −20–80 °C. The battery testing equipment has a variety of working modes, such as cross-current charging and discharging, shelving, cycling, and simulation steps. The charging and discharging currents of the battery are controlled by BTS7.6.0 software to simulate the mode

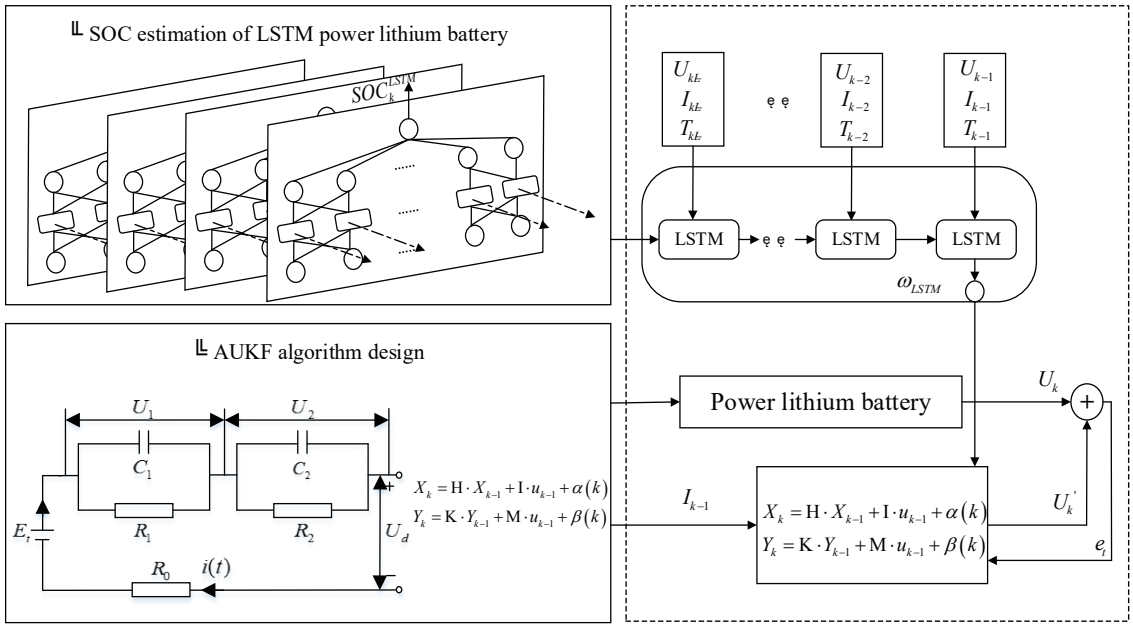

Fig. 5. Overall flow chart of SOC estimation method for power lithium battery based on LSTM–AUKF fusion algorithm.

Table 1
Performance parameters of battery.

Description	Value
Size (mm^2)	18 × 65
Nominal capacity (mAh)	1500
Nominal voltage (V)	3.2
Charge cutoff voltage (V)	3.65
End-of-discharge voltage (V)	2.5
Ohmic internal resistance (Ω)	28
Discharge maximum continuous current (A)	2
Working temperature (°C)	25

of the battery at different temperatures and under different driving conditions, and to record the current and voltage data of the battery at the same time.

Charging and discharging devices are mainly used to control the charging and discharging powers and currents of the battery. The current, voltage, power, and other parameters of the monitored battery are transferred to the upper computer system through a local area network. A temperature and humidity control box is used to set the ambient temperature in the experiment, which enables the battery to be tested under the required ambient temperature and humidity conditions to ensure the validity of the test. The upper computer system is used to detect and record the changes in various parameters of the battery and the sampling time. For the SOC–OCV test and multi-condition random charge and discharge simulation of different battery levels, the test equipment of the corresponding level should be configured to measure the test

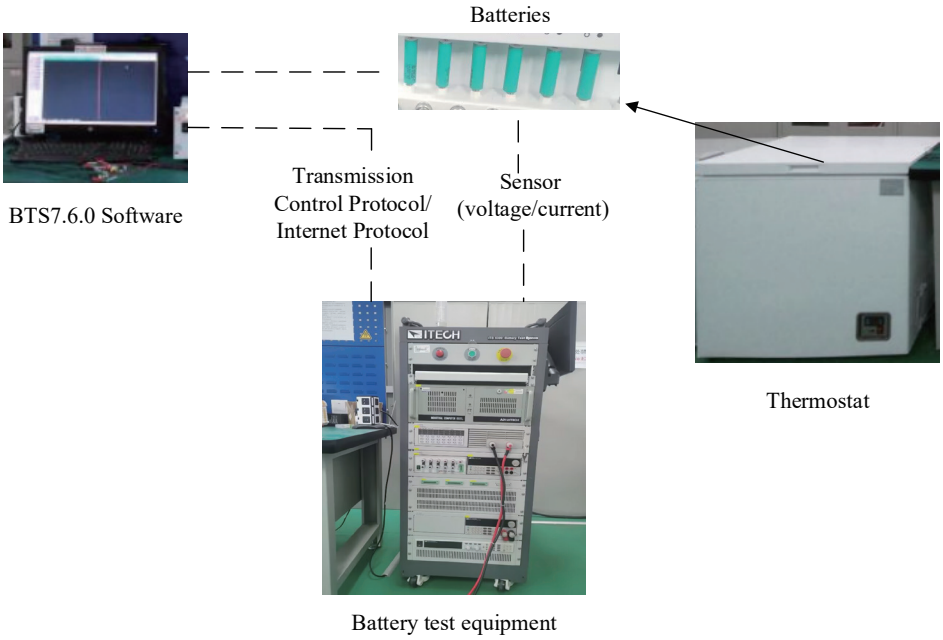

Fig. 6. (Color online) Experimental test platform.

data of battery working condition feedback. For power lithium battery levels, the corresponding equipment should be configured.

4.2 Calibration of SOC–OCV–T functional relationships

In batteries, one OCV value corresponds to one SOC value; thus, obtaining the relationship between them plays an important role in the estimation of the SOC for batteries. The selected batteries are tested under SOC–OCV operating modes, and the SOC–OCV relationship is obtained from the OCV. The average OCV in the charge and discharge directions under the same SOC value is obtained, and then the SOC–OCV relationship curve is fitted with a sixth-degree polynomial. When the batteries are fully charged, pulse discharge tests are performed at a discharge rate of 0.5 C and temperatures of 0, 25, and 45 °C. The SOC–OCV–T relationship shown in Fig. 7 is plotted using the data collected from the experimental equipment. The SOC–OCV relationship varies with the temperature. This indicates that battery characteristics are affected by temperature, which in turn affects the SOC estimation.

4.3 Experiments and data analysis

4.3.1 SOC estimation error

To verify its estimation accuracy, the LSTM–AUKF algorithm is compared with the UKF algorithm under different operation modes. The initial SOC value used in the algorithm is 80% and the actual SOC is 90%. Figure 8 shows a comparison of different algorithms for estimating

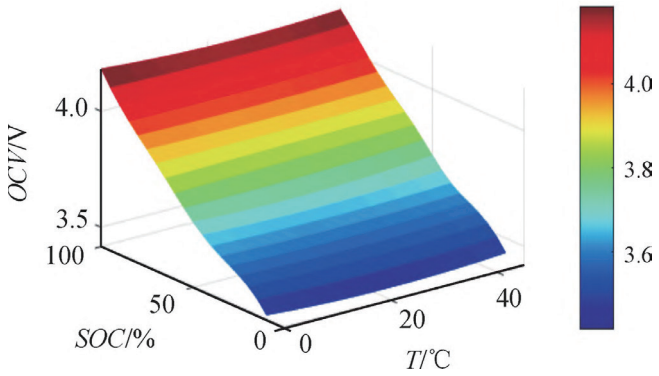

Fig. 7. (Color online) SOC–OCV–T relationship.

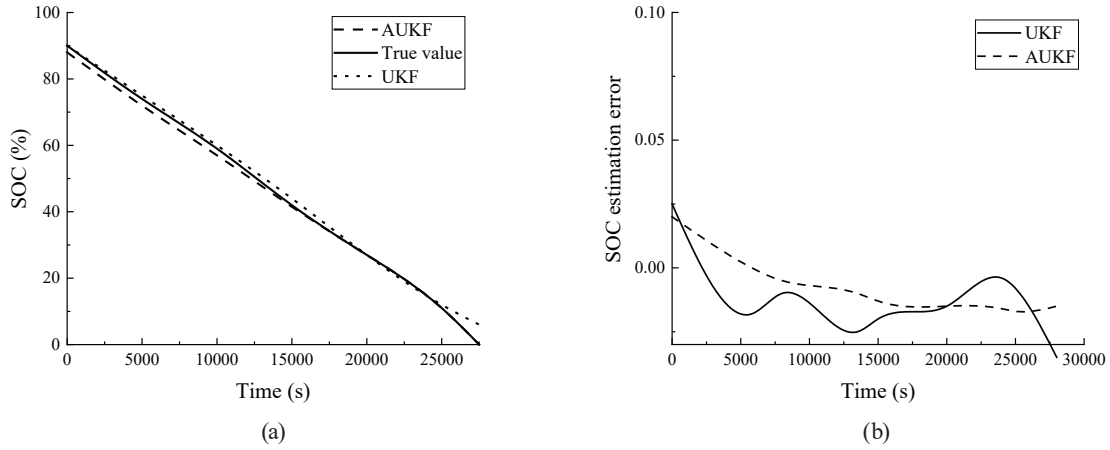

Fig. 8. Comparison of SOC under DST operating conditions. (a) SOC estimation results. (b) SOC estimation error.

the SOC under dynamic stress test (DST) operating conditions. It can be seen that the estimation accuracy of the two algorithms decreases with increasing depth of the discharge. Overall, the LSTM–AUKF algorithm has superior accuracy, stability, and convergence of estimation to the UKF algorithm; thus, it more closely reflects the true SOC value. The RMSE values of the UKF and LSTM–AUKF algorithms are 1.58 and 2.01%, respectively. Figure 9 shows a comparison of the two algorithms for estimating the SOC under Federal Urban Driving Schedule (FUDS) operating conditions. It can be seen that the estimation errors of the two algorithms are relatively small under complex modes. However, the difference between the estimated SOC value obtained by the LSTM–AUKF algorithm and the real SOC value is smaller than that for the UKF algorithm. When the initial SOC deviates from the real SOC, the estimated SOC more rapidly converges to the actual value for the LSTM–AUKF algorithm. The estimation results show that the LSTM–AUKF algorithm has a significantly higher performance than the UKF algorithm. The RMSE values of the UKF and LSTM–AUKF algorithms are 1.82 and 1.02%, respectively. From Figs. 8 and 9, the LSTM–AUKF algorithm has a higher performance than the UKF algorithm in terms of estimation accuracy, convergence, and stability when the initial SOC is biased and the system noise is unknown. In addition, the LSTM–AUKF algorithm controls the

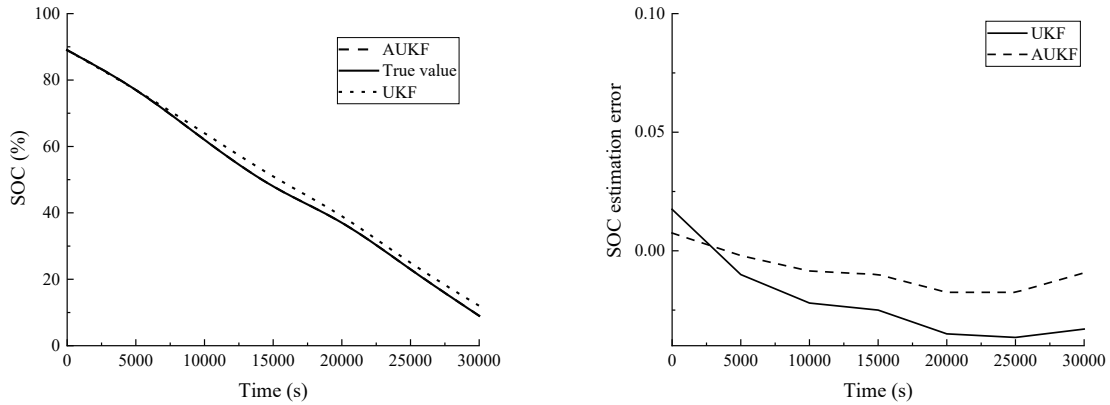

(a) (b)

Fig. 9. Comparison of SOC under FUDS operating conditions. (a) SOC estimation results. (b) SOC estimation error.

Table 2
Comparison of convergence times for different algorithms with different SOC initial errors.

Initial error (value) of SOC (%)	Optimization window LSTM (s)	Optimization window LSTM–EKF (s)	Optimization window LSTM–AUKF (s)
5 (95)	108	96	32
10 (90)	124	115	39
15 (85)	169	132	46
20 (80)	175	181	47

RMSE value to less than 1.1%. These results clearly verify the advantageousness of the LSTM–AUKF algorithm in SOC estimation.

4.3.2 Convergence time for SOC estimation

The convergence time *Tr* values of different fusion algorithms are next tested for different errors of the initial SOC value (the true SOC is 100% and the initial value is set to 95, 90, 85, or 80%). When the initial SOC errors are 5, 10, 15, and 20%, the *Tr* values of the optimization window LSTM–AUKF algorithm are 32, 39, 46, and 47 s, respectively. These values are 76, 85, 123, and 128 s smaller than those of the optimization window LSTM–EKF algorithm and 64, 76, 86, and 134 s smaller than those of the optimization window LSTM–EKF algorithm. Therefore, *Tr* is smallest for the optimization window LSTM–AUKF algorithm, and this algorithm performs higher than the other two algorithms for different initial SOC errors (Table 2).

5. Conclusions

This paper presents a method of estimating the SOC of power batteries that is based on the LSTM–AUKF fusion algorithm. The main contribution of this study is the construction of a method of estimating the SOC of LIBs using the optimization window LSTM–AUKF fusion algorithm. By analyzing the characteristics of the window LSTM depth network and AUKF

algorithm, the optimization window LSTM–AUKF fusion algorithm is proposed. It is divided into two key steps: an optimization window LSTM–AUKF fusion algorithm for LSTM network estimation and Cholesky decomposition adjustment for windows, which can improve the estimation accuracy of the SOC. We built a platform to test the SOC estimation of a power battery under charging and discharging conditions, and we compared the SOC estimation error and convergence time between different algorithms. Experimental results show that the RMSE, MAX, and MAE of the proposed optimization window LSTM–AUKF algorithm are 1.13, 1.74, and 0.39%, respectively. Compared with the LSTM and LSTM–EKF estimation algorithms, the LSTM–AUKF estimation algorithm clearly has superior performance in terms of MAX and MAE as well as a short convergence time.

Acknowledgments

This work was supported by the Science and Technology Research Program of Chongqing Municipal Education Commission (Grant KJQN202003501).

References

1 Y. Gao, K. Liu, C. Zhu, X. Zhang, and D. Zhang: IEEE Trans. Ind. Electron. **69** (2022) 2684. https://doi.org/10.1109/TIE.2021.3066946
2 W. Zhang, L. Wang, L. Wang, C. Liao, and Y. Zhang: IEEE Trans. Ind. Electron. **69** (2022) 3677. https://doi.org/10.1109/TIE.2021.3073359
3 M. O. Qays, Y. Buswig, M. L. Hossain, and A. Abu-Siada: CSEE J. Power Energy Syst. **8** (2022) 105. https://doi.org/10.17775/CSEEJPES.2019.03060
4 P. Xu, X. Hu, B. Liu, T. Ouyang, and N. Chen: IEEE Trans. Ind. Inf. **18** (2022) 6150. https://doi.org/10.1109/TII.2021.3131725
5 S. Song, H. Wei, Y. Lin, C. Wang, and A. Gómez-Expósito: J. Mod. Power Syst. Clean Energy **10** (2022) 627. https://doi.org/10.35833/MPCE.2020.000613
6 K D. Rao, S. Ghosh, and M. R. Kumar: IEEE Trans. Ind. Appl. **57** (2021) 5264. https://doi.org/10.1109/TIA.2021.3089456
7 Q. Zhang, C. Huang, H. Li, G. Feng, and W. Peng: IEEE Trans. Transp. Electrif. **8** (2022) 4633. https://doi.org/10.1109/TTE.2022.3160021
8 K. D. Rao, S. Ghosh, and R. Keshri: IEEE Trans. Energy Convers. **37** (2022) 1600. https://doi.org/10.1109/TEC.2022.3144478
9 R. Guo and W. Shen: IEEE Trans. Veh. Technol. **71** (2022) 11515. https://doi.org/10.1109/TVT.2022.3193735
10 H. Aung, J. J. Soon, S. T. Goh, J. M. Lew, and K.-S. Low: IEEE Trans. Aerosp. Electron. Syst. **56** (2020) 2978. https://doi.org/10.1109/TAES.2019.2958161
11 L. M. Caro, G. Ramos, K. Rauma, D. F. C. Rodriguez, D. M. Martinez, and C. Rehtanz: IEEE Trans. Ind. Appl. **57** (2021) 2077. https://doi.org/10.1109/TIA.2021.3057350
12 P. Shrivastava, T. K. Soon, M. Y. I. B. Idris, S. Mekhilef, and S. B. R. S. Adnan: IEEE Trans. Veh. Technol. **70** (2021) 1200. https://doi.org/10.1109/TVT.2021.3051655
13 Y. Wu, Q. Wang, J. Liu, C. Zhao, H. Tang, and K. Kang: IEEE Microwave Wireless Compon. Lett. **28** (2018) 804. https://doi.org/10.1109/LMWC.2018.2850895
14 J. Pan, Z. Tan, X. Wang, L. Nie, C. Sha, and X. Chen: IEEE Trans. Plasma Sci. **43** (2015) 557. https://doi.org/10.1109/TPS.2014.2385877
15 Y. Wang, X. Han, D. Guo, L. Lu, Y. Chen, and M. Ouyang: IEEE J. Radio Freq. Identif. **6** (2022) 968. https://doi.org/10.1109/JRFID.2022.3211841
16 S.-T. Yun and S.-H. Kong: IEEE Trans. Aerosp. Electron. Syst. **58** (2022) 5292. https://doi.org/10.1109/TAES.2022.3167624
17 R. Jin, Z. Chen, K.Wu, M. Wu, X. Li, and R. Yan: IEEE Trans. Instrum. Meas. **71** (2022) 1. https://doi.org/10.1109/TIM.2022.3167778

About the Authors

Mingcan Xu received his B.S. degree from Chongqing Three Gorges University, China, in 2003. He was a visiting scholar at Singapore Nanyang Polytechnic, Singapore, and Technical University of Dresden, Germany, in 2013 and 2019, respectively. He joined Chongqing Three Gorges Vocational College in 2003, where he is currently an associate professor. His research interests include electronic information engineering, the application of electronic and communication engineering, and automation. (2011190235@cqsxzy.edu.cn)

Yong Ran received his B.S. degree in electronic information engineering from Chongqing Three Gorges University in 2003 and his M.S. degree in signal and information processing from University of Electronic Science and Technology in 2010. He is currently an associate professor with College of Intelligent Manufacturing, Chongqing Three Gorges Vocational College. His research interests include intelligent signal processing and wireless sensor networks. (xumc107@163.com)